Force Balance Calibration and the Modern Design of Experiments

By

George R. Moll III

(Under the Direction of R. Benjamin Davis)

Abstract

The University of Georgia High-Speed Water Tunnel (HSWT) is a closed-loop water tunnel primarily used to study fluid-structure interaction. A force balance is used to measure forces on models within the HSWT. The force balance is a key instrument in many hydrodynamic experiments, so it is necessary to design a robust calibration process for the balance. This thesis documents the development of a calibration experiment that follows the Modern Design of Experiments (MDOE) methodology. MDOE is a process for designing, executing, and analyzing experiments using quality assurance techniques to guard against systematic error. To validate the calibration, the balance is used to compute lift and drag coefficients for a plate at various angles of attack. Predictions made with the balance were consistent with published results, indicating that the instrument is reliable. This investigation is relevant because improving the force balance increases the capabilities of the water tunnel.

Index Words: Modern Design of Experiments, force balance, calibration, blocking, randomization, replication

Force Balance Calibration and the Modern Design of Experiments

By

George R. Moll III

B.S.M.E., The University of Georgia, 2019

A Thesis Submitted to the Graduate Faculty
of The University of Georgia in Partial Fulfillment
of
the Requirements for the Degree

Masters of Science

Athens, Georgia

2020

Force Balance Calibration and the Modern Design of Experiments

By

George R. Moll III

Major Professor: R. Benjamin Davis

Committee: Beshoy Morkos
C. Brock Woodson

Electronic Version Approved:

Ron Walcott
Dean of the Graduate School
The University of Georgia
December 2020

Acknowledgments

I am proud to be a graduate of the University of Georgia, and I want to thank the faculty and staff of the College of Engineering that contributed to my undergraduate and graduate experiences. I would especially like to thank my advisor, Dr. R. Benjamin Davis, for giving me inspiration, opportunity, and guidance. My proudest moments as a student at the University of Georgia all involve working with him. I am grateful to Dr. Morkos and Dr. Woodson for serving on my Master's Advisory Committee. I've had the pleasure of taking their courses, and their feedback on my thesis was illuminating. I would also like to thank my labmates, especially Bianca Bitere, for helping me navigate graduate school, tackle research questions, and clean up if I overfill the water tunnel.

This thesis would not have been possible without the support of my incredible parents, George and Cathy Moll. This work is dedicated to them and to Thomas Andrew Morrow.

Contents

List of Tables

List of Figures

Chapter 1

Introduction

1.1 Overview

The Dynamic Devices and Solutions Lab (DDSL) houses the University of Georgia High Speed Water Tunnel (HSWT). Analogous to wind tunnels, water tunnels are often used for hydrodynamic characterization and flow visualization studies because they allow for close control over a flow environment. A strain gage force balance is used to identify flow-induced loads on test articles within the HSWT, and it is necessary to design a high quality calibration process for the instrument. This project aims to evaluate the current DDSL force balance design through calibration experiments and better understand the instrument's reliability.

1.2 Thesis Scope

This thesis details the design of a calibration process for a multi-piece external force balance and its use in a hydrodynamic investigation. The document is organized as follows:

- **Chapter 2:** This chapter covers the HSWT, force balance usage, One Factor at a Time (OFAT) experiments, and Modern Design of Experiments (MDOE).
- **Chapter 3:** Instrumentation is discussed in this chapter. The original force balance design and recent modifications are detailed.
- **Chapter 4-6:** Chapters 4 - 6 are organized by the distinct phases of MDOE. Chapter 4 covers the design phase where data volume is determined. Chapter 5 details the experiment and relevant lab techniques, and Chapter 6 includes all of the post-processing.
- **Chapter 7:** The verification plate test is detailed here.
- **Chapter 8:** Conclusions are provided.

Chapter 2

Background

2.1 UGA High Speed Water Tunnel

The UGA HSWT is a variable pressure closed-loop water tunnel designed for hydrodynamic testing. The design incorporates elements from the U.S. Navy's Large Cavitation Channel (LCC) and the University of New Hampshire's High-Speed Cavitation Tunnel (HiCaT) [1–3]. The test section measures 12" x 12" x 39.4" with a maximum recorded flow speed of 40.0 ft/s. To date, the facility has been used to investigate a variety of phenomena including: underwater flutter, vortex energy capture, vortex induced vibration, and hydroelastic damping.

Figure 2.1. View of HSWT, mezzanine, and water storage tank [1]

2.2 Force Balances

Balances are force transducers made of flexures that deflect when loaded. They are used in hydrodynamic and aerodynamic testing to measure flow-induced loads on test articles. The earliest balances were mechanical, measuring loads using weight scales, but now most force balances have electrical elements that relate applied loads to voltage signals. A balance can be described by how many forces it can measure, how it interfaces with the test article, how many pieces it is made of, and the type of strain gages it uses. Six-component balances are the most complex, capable of measuring three axial forces (normal, side, and axial) and three moments (pitch, yaw, and rolling).

Monolithic force balances machined from a single block of material behave differently than non-monolithic balances made from multiple pieces mechanically fastened together [4, 5]. Monolithic balances have a continuous response when the load polarity changes, but the response from an assembled force balance may spike or change slope at the zero load point. The American Institute of Aeronautics (AIAA) states "...it is not uncommon for the

load/output relationship of balances, especially those of multi-piece design, to exhibit some dependency on the sign of the strain in the measuring elements." [5]. The recommended math model represents strain gage signals as polynomial functions of component loads. The most common math model used to describe the load/output relationship for balances is a second-order polynomial of the form:

$$R_i = a_i + \sum_{j=1}^{n} b_{i,j} F_j + \sum_{j+1}^{n} \sum_{k=j}^{n} c_{i,j,k} F_j F_k, \tag{2.1}$$

where R_i is the voltage signal for the i^{th} component related to single and two-component loads F_j and F_k [5]. The recommended practice to model asymmetric behavior in the response is to include absolute value terms in the response surface model. Equation 2.1 extended to include cubic and absolute value terms becomes:

$$\begin{aligned} R_i = a_i &+ \sum_{j=1}^{n} b_{1i,j} F_j + \sum_{j=1}^{n} b_{2i,j} |F_j| + \sum_{j=1}^{n} c_{1i,j} F_j^2 + \sum_{j=1}^{n} c_{2i,j} F_j |F_j| \\ &+ \sum_{j=1}^{n} \sum_{k=j+1}^{n} c_{3i,j,k} F_j F_k + \sum_{j=1}^{n} \sum_{k=j+1}^{n} c_{4i,j,k} |F_j F_k| + \sum_{j=1}^{n} \sum_{k=j+1}^{n} c_{5i,j,k} F_j |F_k| \\ &+ \sum_{j=1}^{n} \sum_{k=j+1}^{n} c_{6i,j,k} |F_j| F_k + \sum_{j=1}^{n} d_{1i,j} F_j^3 + \sum_{j=1}^{n} d_2 i, j |F_j^3|. \end{aligned} \tag{2.2}$$

This model is referred to as the "iterative model" [5]. Coefficients are classified by [5]:

- "offset" a_i
- first-order coefficient, b_i
- second-order coefficients, $c_{i,j,k}$
- third-order coefficients, $d_{i,j}$

Various alternative models exist, each with unique benefits and drawbacks. The independent model approach suggests using separate regression models and experimental designs for each sub-region [4]. A second-order response surface model is built for each sub-space with the form:

$$R_i = a_i + \sum_{j=1}^{n} b_{i,j} F_j + \sum_{j=1}^{n} c_{1i,j} F_j^2 + \sum_{j+1}^{n} \sum_{k=j}^{n} c_{2i,j,k} F_j F_k. \tag{2.3}$$

This approach requires a conditional statement in the MATLAB script based on the sign of the applied forces to use the correct RSM to estimate loads. Because the method performs a least squares regression (LSR) in one sub-region, only points within that region can be used in a lack of fit analysis [4]. This method was chosen to calibrate the DDSL force balance because the RSM model is the standard for MDOE calibration at NASA LaRC [6], and the current design does not allow the force balance to be loaded with negative and positive forces in the same design space without re-positioning and rewiring the balance.

External balances are placed outside of the test article, making them flexible to use, but they always add some level of influence to the fluid flow about a test article. Internal balances are placed inside of the model, which does not influence fluid flow, and are commonly used in wind tunnel testing. Using FEA simulations, Robinson found that for a re-entry type configuration superior accuracy of the recovered force and moment loads was obtained with an external force balance rather than an internal balance [7]. He hypothesized it was due to increased balance stiffness and decoupling between force components that can be achieved with an external configuration. The DDSL uses an external balance placed outside of the test section. The design allows test articles to be easily installed, and the model can be rotated about a rod that passes through the center of the balance without draining the test section. The specifics of the DDSL force balance are discussed in later chapters.

2.3 Modern Design of Experiments (MDOE)

Conventional experimental procedures follow the On Factor At a Time (OFAT) method, in which all but one of the independent variables are held constant, while one factor is systematically changed at uniform intervals. Responses are measured at each level of the chosen factor. This process is repetitive; each variable of interest is incremented until all combinations have been set. MDOE pioneered by Richard DeLoach was developed at NASA Langley Research Center (LaRC) as an alternative to classical experiment designs associated with OFAT testing. The motivation behind its development was the process-oriented challenges facing the aeronautical research community at the turn of the century [8]. At the time, quantifiable criteria for an acceptable process outcome in experimental aeronautical research were rarely defined. Researchers opted to use all available test resources to avoid stopping before collecting an adequate volume of data, which made the research costlier than necessary [8]. MDOE focuses on obtaining scientifically defensible answers to specific research questions with the smallest amount of data necessary. The process involves a design phase, execution phase, and analysis phase [8]. In the design phase, data volume is determined based on precision requirements, acceptable inference error risk, and repeatability of the test environment, and variable combinations are selected to minimize the uncertainty in predictions made from response surface models [8–11]. Blocking, randomization, and replication are tactics used in the execution phase to minimize uncertainty and collect quality data [8,12–15]. In the analysis phase, response surface models are developed to estimate the mathematical relationships among dependent and independent variables.

2.3.1 Blocking

Blocking identifies and reduces error attributable to effects over time, which typically represent a significant amount of the total unexplained variance in wind and water tunnel testing.

These effects are due to instrument drift, temperature changes, and other factors that can negatively impact the reproducibility of test results. The blocking technique involves grouping data points into "blocks" which are executable in a short amount of time. The mean of replicates in one block are compared to nominally identical replicates in another block to determine if the difference is large enough to detect in the presence of chance variations in the data [10]. If the difference is detectable, it is called a "block effect", and blocking permits the RSM to include a term for block effects. To achieve this, "blocking variables" are assigned to tag the data points according to which blocks they are in. The blocking variables have a constant value for all points within the same block. Consider developing an RSM for a one-component force balance. The RSM would be a function of the component force and block. If a second-order polynomial is a sufficient model it would look like:

$$R = b_0 + b_1 x + b_2 x^2 + cz, \tag{2.4}$$

where x represents the component load and z represents the coded blocking variable. Say this is a two-block experiment, with one block assigned a blocking variable of 1, and the other is assigned a blocking variable of -1. Equation 2.4 could then be written as

$$R = (b_0 \pm c) + b_1 x + b_2 x^2. \tag{2.5}$$

The coefficient of the blocking variable represents how much the intercept of each block differs from the midpoint between them [10]. The block effect is defined as the change in intercept between the two blocks. Including this in the model converts some unexplained variance in explained variance due to a block effect, and the magnitude of the blocking variable can provide insight into the source of the uncertainty [10].

2.3.2 Randomization

If an independent variable is incremented, time-varying effects will introduce bias between early and late measurements. Fisher recognized this in the early 20th century and showed that setting independent variables in random order defends against systematic variation [16] Consider the one-component force balance from earlier. While calibrating, suppose we randomized the point order to ensure that some of the lower calibration loads were acquired earlier, and some were acquired later. If early measurements are biased low and later measurements bias high, randomization results in the points being randomly distributed about their true unbiased estimate [14]. Randomization is a defense to systematic variation within a sample, and blocking identifies between-sample variation. These techniques decouple unexplained systematic variations from independent variable effects. Systematic error is converted into a component of random error that is easier to correct through replication.

2.3.3 Replication

Replication causes random errors to cancel and provides unbiased estimates of "pure error". Pure-error estimates make it possible to separate unexplained variance into lack-of-fit and pure-error components. This is relevant because if the lack-of-fit is significant, higher-order models can be used to improve balance load estimation quality. Ideally, replicates are acquired at all levels of the factors under study to estimate pure error. Genuine replicates are acquired by repeating a combination after factors have been changed.

Chapter 3

Instrumentation

3.1 Force Balance

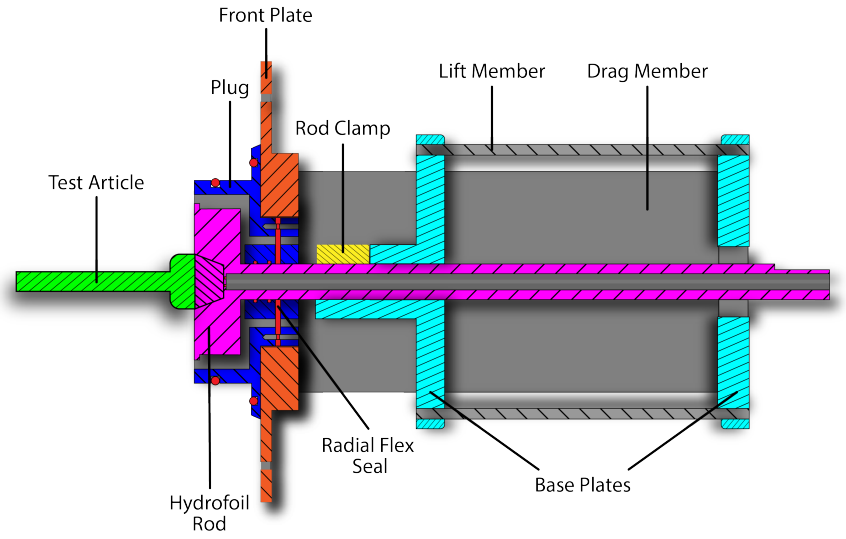

Figure 3.1. Cross-sectional view of force balance [1]

The DDSL uses a modified external force balance design based on one obtained from the University of New Hampshire [17]. The balance is a two-component multi-piece instrument made of a hydrofoil rod connected to bending plates. It mounts to an aluminum window on the test section of the HSWT, and the hydrofoil rod passes through a radial flex seal into the test section (Fig. 3.2). Test articles are mounted to the rod using a key and slot connection. When flow imposes forces on a test article, the radial flex seal allows the hydrofoil rod to deflect, which deforms the bending plates of the force balance. Strain gages on the force balance output a voltage signal proportional to the strain in the cantilevered plates.

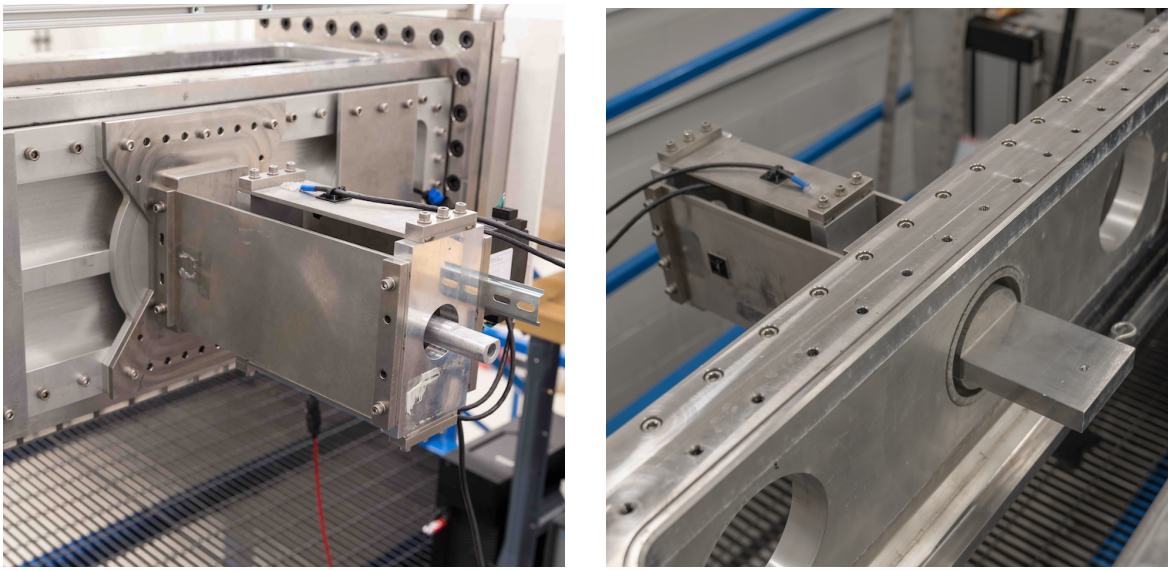

Figure 3.2. (a) Side view of attached force balance and (b) top view of attached force balance [1]

The leads of the strain gages are soldered to shielded wire and secured to bridge terminal plates adhered to the force balance. A layer of silicone protects the strain gages, and cable tie anchors prevent the cable from being pulled. The leads of the shielded wire are connected with ferrules in a full-bridge configuration, and these ends interface with the terminal blocks of an Omega DMD4059 signal conditioner. The signal conditioner and shielded wire reduce the amount of electrical noise in the signal introduced by the motor circulating water in the tunnel.

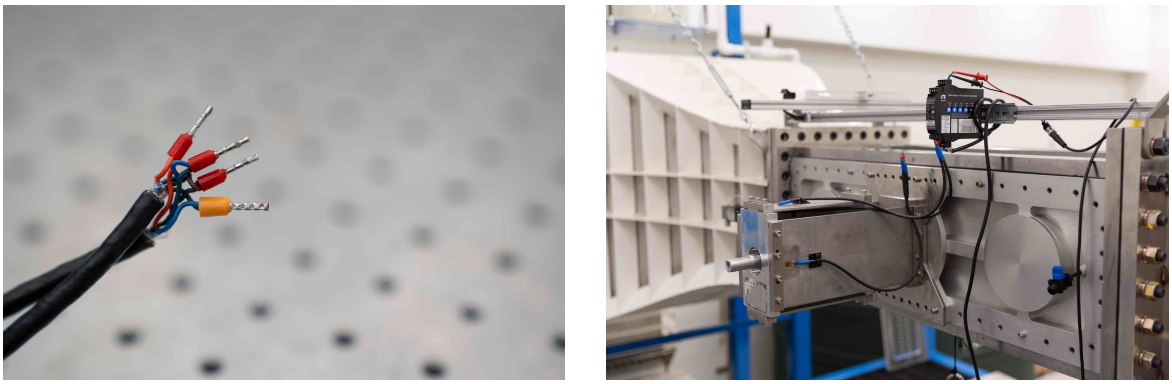

Figure 3.3. (a) Ferrules and (b) force balance wired to signal conditioner [1]

3.1.1 Original Calibration Method

The force balance was initially calibrated by using OFAT methods to obtain two calibration curves in the form of first-order polynomials. Weights were hung from a test block attached to the force balance to simulate lift or drag loads. One variable was held at zero, while the other was systematically changed at random intervals. Responses were measured at each level of the component force. Once all responses were recorded, the wiring to the signal conditioner was changed from one strain gage channel to the other, and the process was repeated. The drag channel was calibrated by rotating the entire force balance assembly 90° to avoid using a pulley system. This configuration will be referred to as the "horizontal" configuration. The force balance was never loaded with lift and drag forces at the same time so the models constructed from the data did not include interactive terms. The first design was capable of handling lift loads up to 960.8 N (216 lbf) and drag loads up to 22.2 N (5 lbf) [1]. The calibration curve for the lift channel is shown in Figure 3.5. Note the strong linear relationship between lift force and the raw mean voltage (RMV) from the strain gages. Figure 3.6 depicts the drag channel responses. When loading the balance in the horizontal configuration with forces greater than 22.2 N, the linear nature of the input/response relationship is lost. Outliers emerge and the trend in the data suggests that load sharing

potentially occurs, thus reducing the force exerted on the bending plates. When unloaded, the balance does not return to a consistent set point like it did for the lift calibration. This is troublesome because it indicates that overloading the force balance in the horizontal configuration in one run will cause the force balance to measure drag forces in subsequent runs that are artificially low.

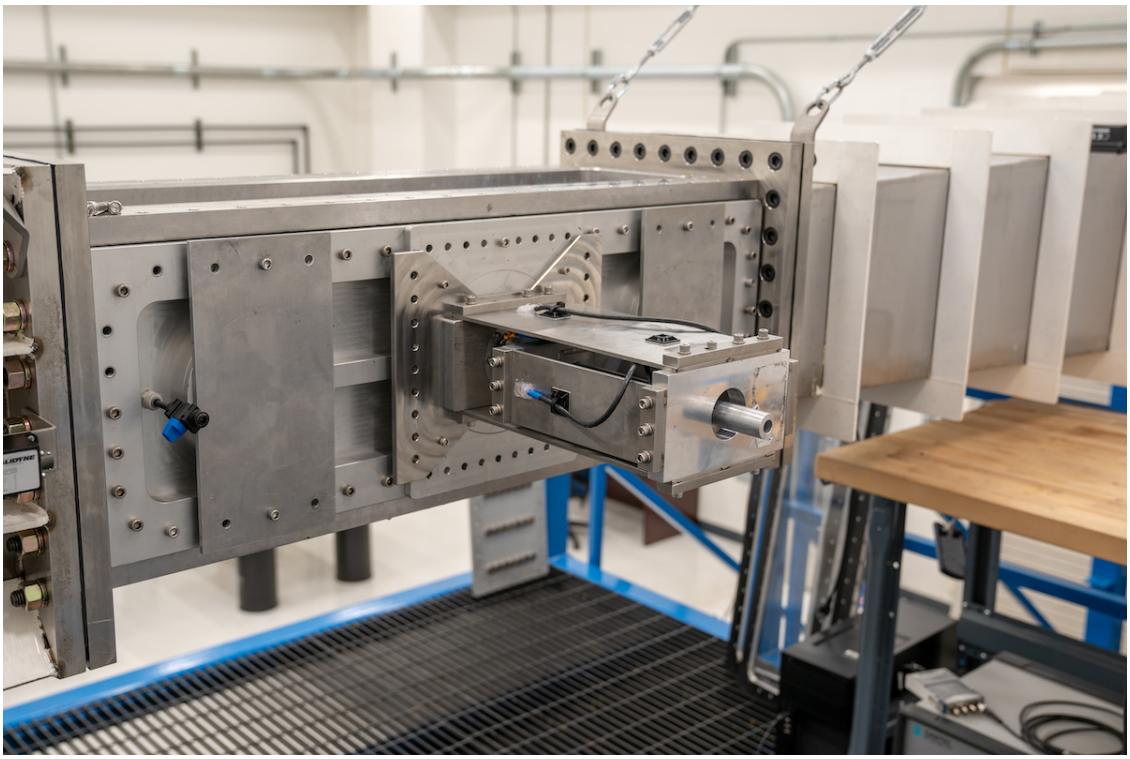

Figure 3.4. Horizontal configuration [1]

To use the instrument in research involving high drag forces, previous operators resorted to leaving the balance in the horizontal configuration during experiments to use the lift plates to support drag loads [1]. The present author used the balance in the horizontal configuration to construct a C_d versus Re plot for a circular cylinder in cross flow to assess this method. An MDOE approach is taken with a modified force balance and discussed later in the thesis, but this initial investigation was done with OFAT techniques.

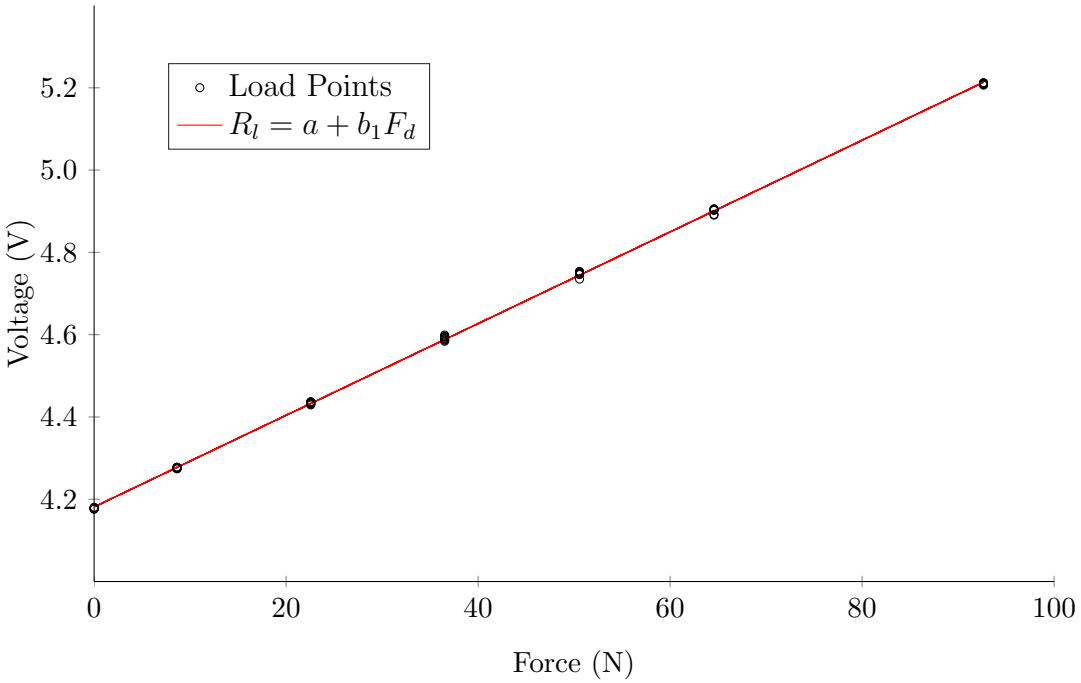

Figure 3.5. First-order lift calibration curve

An acrylic cylindrical test article was attached to the balance and inserted into the test section. "Flow-off" measurements were taken to establish the offset of the unloaded balance. Flow speed in the test section was set in 0.25 m/s increments from 0 to 3.5 m/s, then ramped down by the same increment. Responses were measured at every factor level and converted to force values using the calibration curve shown in Figure 3.5. Re and C_d values were obtained using test article dimensions using the relationships

$$Re = \frac{\rho u D}{\mu} \tag{3.1}$$

and

$$C_d = \frac{2F_d}{\rho A u^2} \tag{3.2}$$

respectively. Results were compared to Weiselsburger's findings as shown in Figure 3.7. Note that the general trend of DDSL results roughly follows those obtained by Weiselsburger

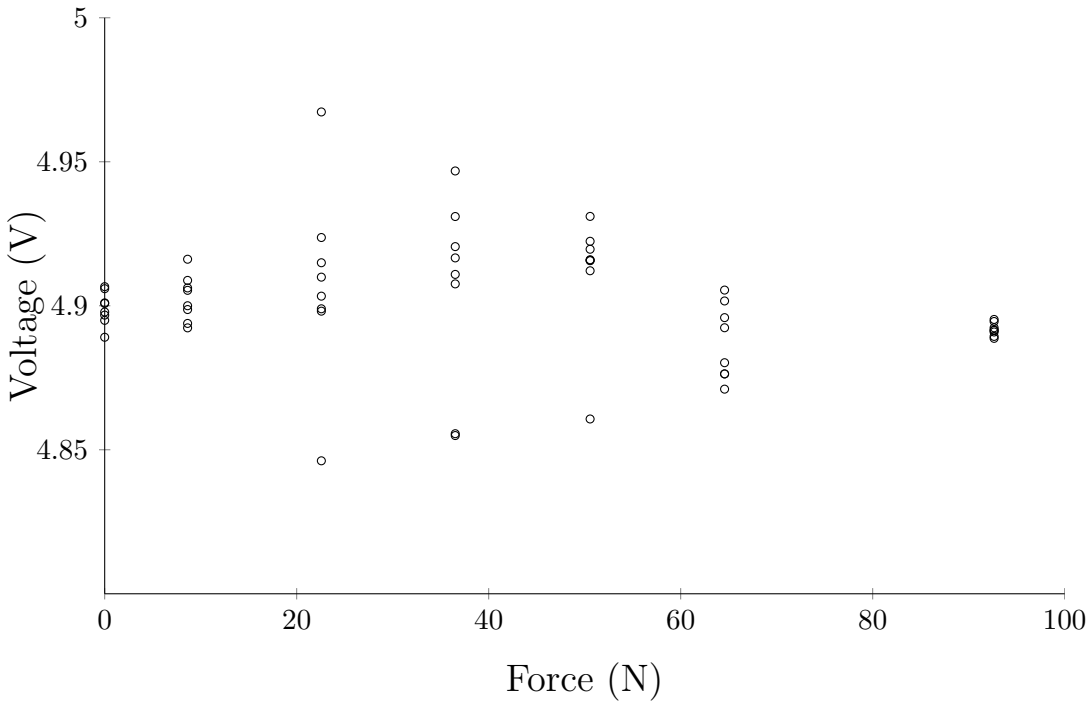

Figure 3.6. Drag calibration results for the original force balance design

[18], but the source of the error is unknown. The first-order calibration curve did not include interactive or higher order terms, and OFAT techniques leave designs susceptible to systematic error.

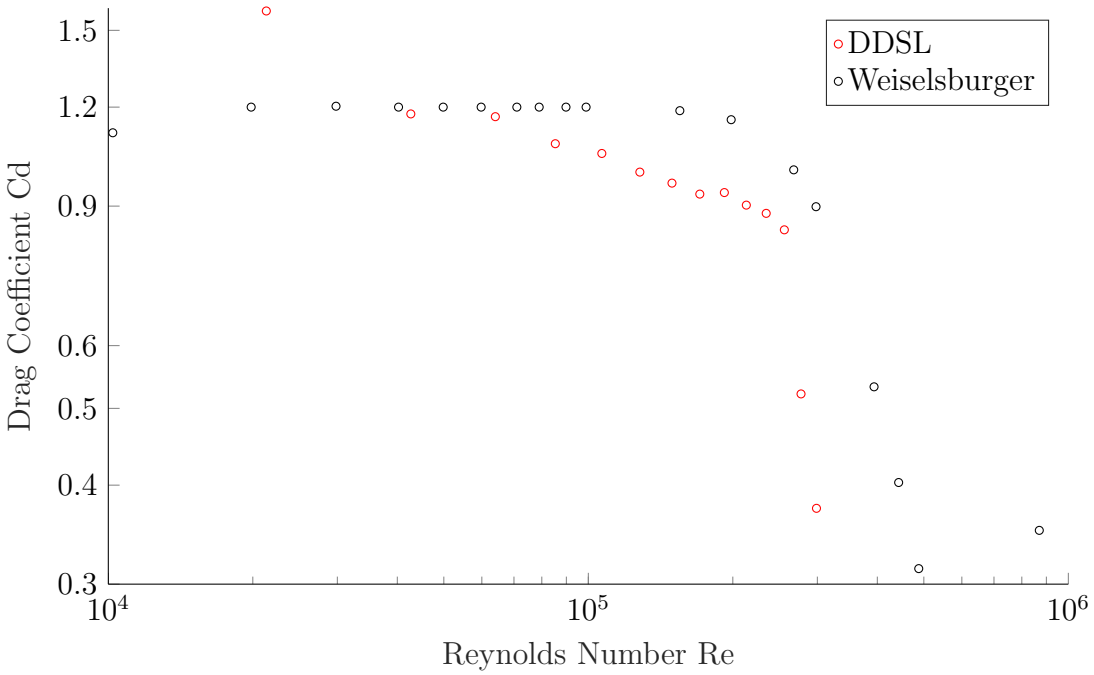

Figure 3.7. Drag coefficient versus Reynolds number

3.2 Force Balance Modifications

MDOE calibration requires the balance to be loaded simultaneously with lift and drag forces. To avoid load sharing in the presence of high drag forces, the stiffness of the balance needed to be increased in the drag direction. Curtis attributed non-linearity in the force balance to the radial flex seal bunching as the force balance approached its maximum capacity [1]. To investigate this, simulations were conducted using Fusion360 to identify how much the hydrofoil rod displaces at the radial flex seal. Note that these models were in a static environment. Under a drag load of 20 N, the hydrofoil rod deflects 0.2318 mm at the location of interest. Increasing the thickness of the drag plates from 3.175 mm to 6.35 mm reduces the displacement to 0.0456 mm as seen in Figure 3.8.

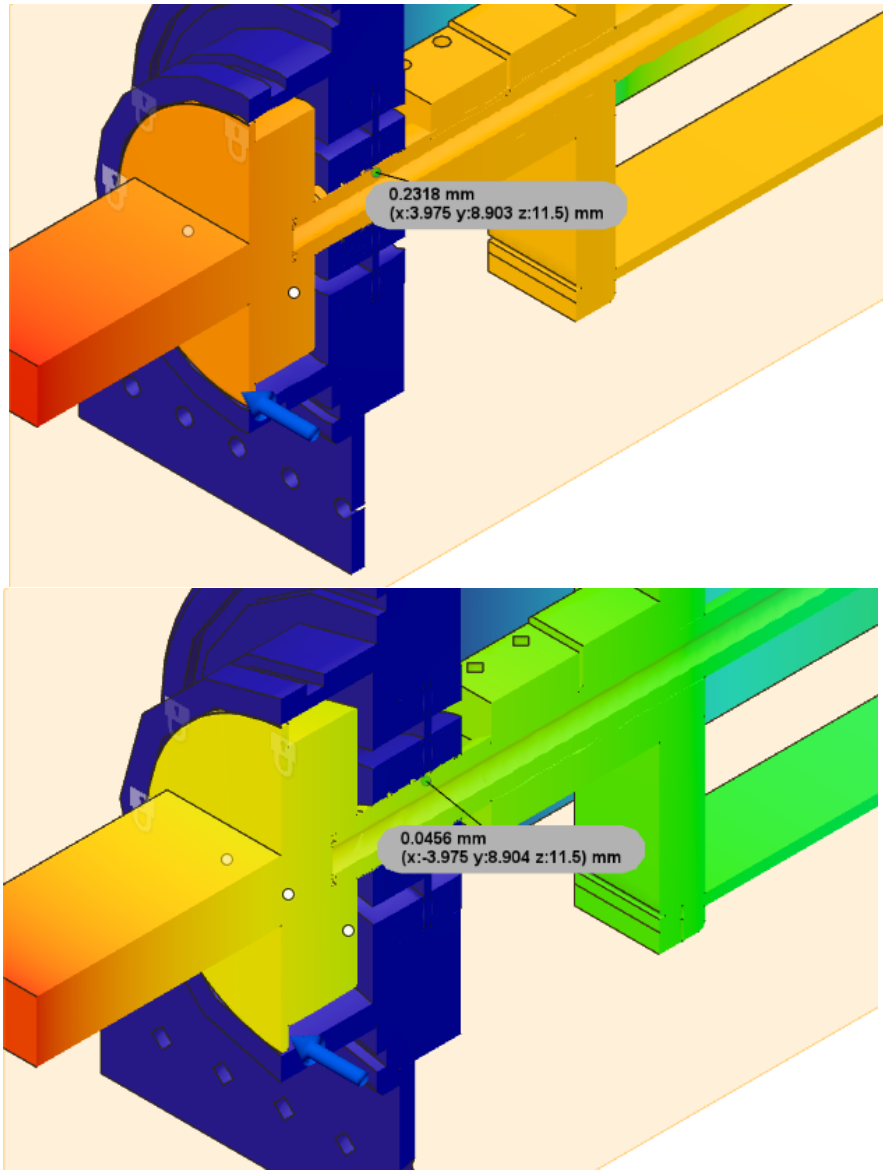

Figure 3.8. Cross-sectional view of force balance with (a) original drag plates and (b) new drag plates under 20 N of drag force

If 20 N does not overload the force balance with the original plates, and the bunching radial flex seal is the source of non-linearity, then the deflection at the point of interest under 20 N is treated as a "critical" displacement. The stiffness of the force balance should be increased such that under greater loads the point of interest does not displace more than the critical displacement. Under 90 N of drag force, the balance with the thicker drag plates

displaces 0.1784 mm, well below the critical value. This increases the stiffness in the drag direction by over 400%.

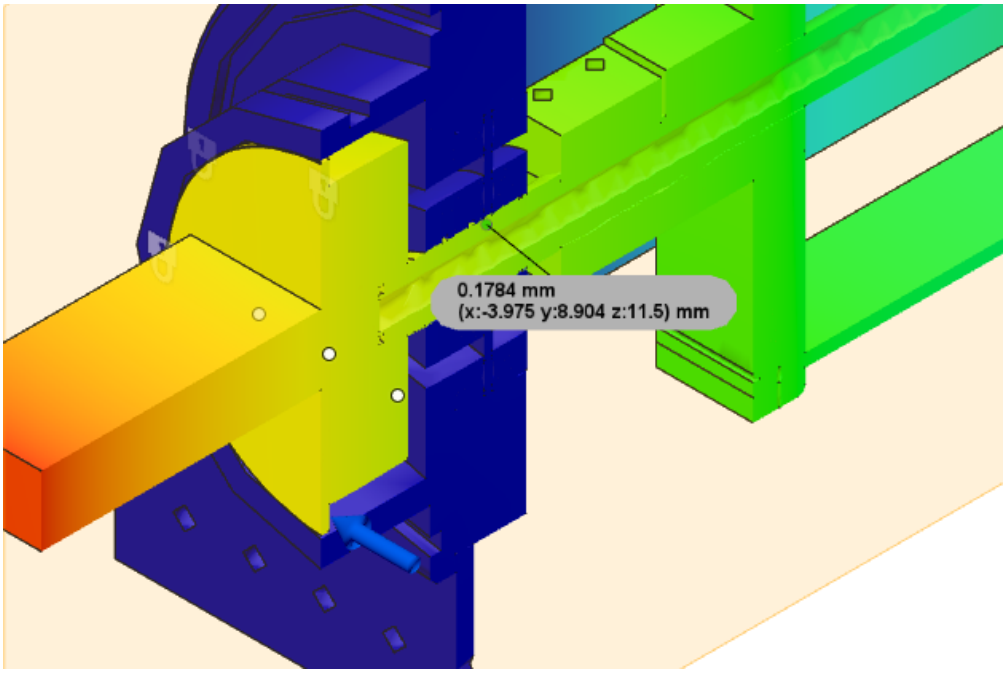

Figure 3.9. Cross-sectional view of force balance with new drag plates under 90 N of drag force

Two 0.25" drag plates were manufactured out of stainless steel, and the surface was polished at the strain gage locations to promote adhesion. The installation area was wiped down with acetone to remove contaminants from the surface. A cold curing cyanoacrylate glue (Loctite 496) was used to secure the strain gages to the plates in a full bridge configuration. The gages were wired following the same process as described above.

3.3 Test Article and Balance Moment Center (BMC)

The test article for the calibration experiment is an aluminum block that bolts to the key and slot interface on the end of the hydrofoil rod. Eyebolts are threaded into tapped holes on the faces of the test block to serve as mounting points for hanging weights. Horizontal loads are

Figure 3.10. View of the test block secured to the force balance [1]

applied to the test article via a pulley system to simulate drag loads. A digital scale is used to verify that the top face of the test block is parallel to the test section, and measurements are taken to position the pulley so that the cable is perpendicular to the vertical face of the test block. A digital spring scale is installed in-line with the horizontal portion of the cable supporting the drag load and the test block. Lift loads are simulated by hanging weights

Figure 3.11. Side view of the pulley system to support calibration weights

vertically from the eyebolt on the bottom face of the test article. Containers made of PVC

are suspended by the cables, and steel BB's are poured into the containers to apply the desired lift and drag loads to the test article.

Figure 3.12. Precision table scale and steel BB's used to load the balance

To calibrate, it is necessary to define the location of the balance moment center (BMC) to resolve component loads into lift and drag forces. The AIAA recommended practice is to place the BMC at the physical center of the force balance, but it can be at any point along the central axis of the balance [5]. Constrained by the existing design, the BMC on the DDSL force balance is placed where the lift and drag force vectors on the test block intersect. The distance between the strain gages and the BMC is important because calibration responses are proportional to the moment created by the loads. The moment center of a test article in a hydrodynamic experiment is different from the BMC, so this must be accounted for to use the calibration curves correctly. If the moment center of a test article is further away from the strain gages than the BMC and this is not considered, force estimates would be greater than their true value.

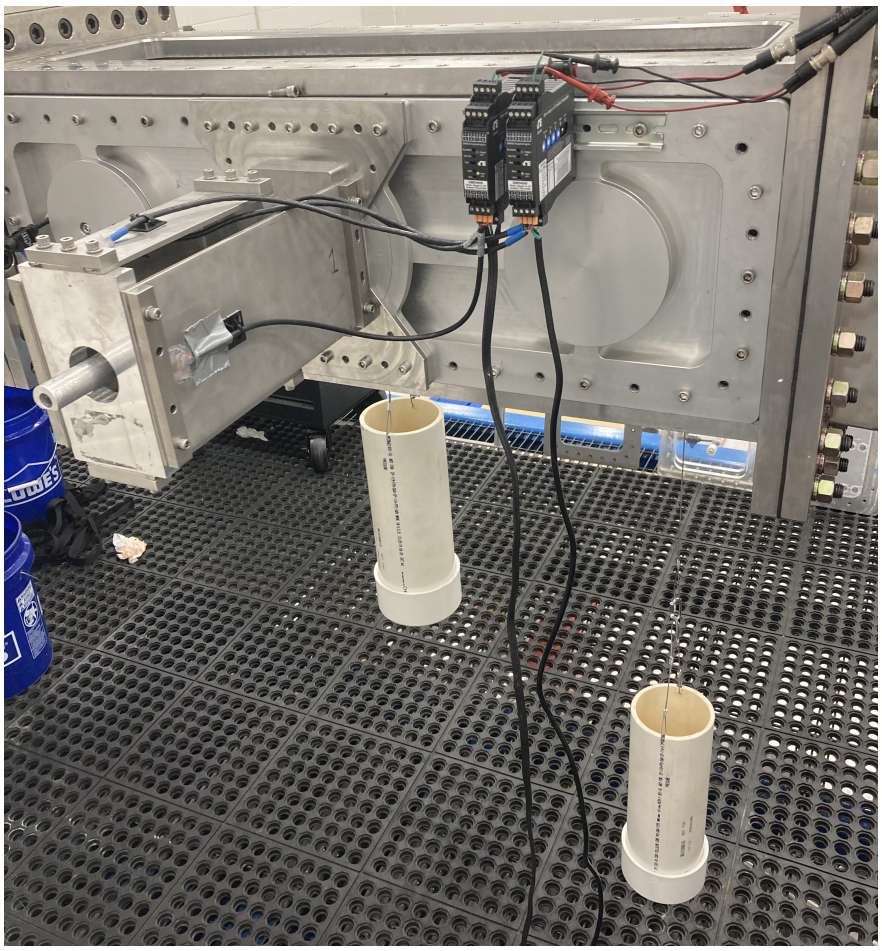

Figure 3.13. Loaded force balance during calibration

Chapter 4

Design Phase

4.1 Data Volume

The calibration is done as a response surface model experiment treating lift and drag loads as independent variables and the raw mean voltage (RMV) outputs of the lift and drag channels of the force balance as response variables. The minimum volume of data required for a polynomial function is based on the equation

$$p = \frac{(d+k)!}{d!k!}, \tag{4.1}$$

where p is the number of parameters in the polynomial, d is the order of the polynomial, and k is the number of variables. Second-order polynomials are widely accepted in the wind tunnel balance community as sufficient models [5]. For a second-order polynomial with two independent variables, the minimum volume of data for each surface response model is equal to the number of parameters, $p = 6$. There are various reasons to collect more than the minimum volume of data, however. Precision requirements, acceptable inference error risk,

and the repeatability of the test environment influence the data volume necessary to obtain the desired math model [11].

4.1.1 Scaling the Experiment

The equation used to scale the volume of data is [11]:

$$N = p(z_\alpha + z_\beta)^2 \left(\frac{\sigma}{\delta}\right)^2 \tag{4.2}$$

where p is the number of parameters from Eq. (4.1), z_α and z_β are the z-statistics pertaining to inference error risk, σ is the repeatability of the test environment, and δ is the prescribed precision requirement. The standard confidence interval reported for balance calibration is 95%. This means that the operator accepts a 5% chance that the model predicts a response that is beyond the precision requirement. For there to be a 95% probability that the two-component force balance is within specification, the probability of any one component being within specification must be:

$$P = 0.95^{0.5} = 0.9747 \tag{4.3}$$

The values for α, β, and the associated z statistics for $P = 0.9747$ are documented in Table 4.1.

Horizontal loads on the test article are measured with an in-line scale to accommodate the calibration pulley system, so the repeatability of the test environment is dependent on the resolution of the in-line scale, which is 0.011 lbf. The precision requirement δ was chosen to be 0.025 lbf, which is 0.10 % of full-scale. The load scale was chosen to be 25 lbf for both lift and drag channels based on the region of operation for the plate verification test.

Table 4.1. Variable values for Equation 4.2

Variable	Drag	Lift
σ	0.011	0.011
δ	0.0250	.0250
α	0.0253	0.0253
β	0.0506	0.0506
z_α, z_β	1.906	1.906

Based on Eqn. 4.2 and the values in 4.1, 17 load combinations are needed to construct second-order RSMs for both the lift and drag channels.

4.2 Design Space

The region over which the calibration is performed is called the design space. The region of operability is the region in which the force balance will be used in the water tunnel. Using the model to extrapolate increases error in the predictions, so it is important that the design space contains the region of operability. The balance was calibrated to predict drag loads (F_l) up to 25 lbf and lift loads (F_d) between -25 and 25 lbf. The force balance was not calibrated for negative drag loads because there are currently no tests involving negative drag in the DDSL.

Latin hyper-cube sampling (LHS) was used to distribute parameters in the design space. LHS is an alternate to Monte Carlo sampling that is widely used in computational applications. LHS can provide a more accurate estimate of the mean value of the math model than Monte Carlo sampling, but it was primarily chosen because LHS allows the user to tailor the number of samples in the design space [19]. This is useful for the calibration because

the number of load combinations is dependent on Eqn. 4.2. Recall that multi-piece balances often behave such that the load/output relationship is asymmetric, so separate regression models and experimental designs were used for each sub-region. The sub-region for positive F_d and negative F_l will be referred to as SR1, and the sub-region for positive F_d and positive F_l is referred to as SR2. Consider the loads for SR1. The range of F_d and F_l are [0,25] lbf and [-25,0] lbf, respectively. For $N = 17$ load combinations, the ranges of F_d and F_l are divided into N "bins" of equal probability, yielding 17^2 total bins in the design space. LHS randomly generates samples (load combinations) with two restrictions: (1) each sample is randomly placed inside of a bin, and (2) for all one-dimensional projections of the 17 samples and bins, there will be only one sample in each bin [19]. The parameters for SR1 are illustrated in Fig. 4.1.

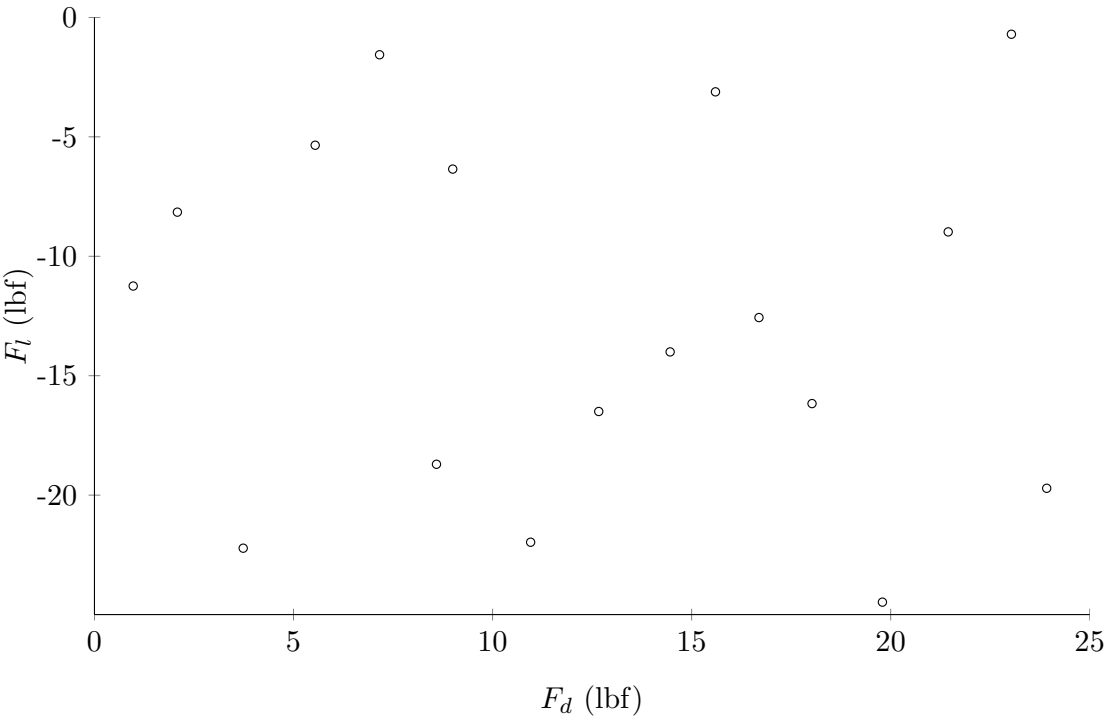

Figure 4.1. Parameter distribution in SR1 using LHS

One drawback to how LHS distributes samples is that the extremes of the design space can be underpopulated. Note in Fig. 4.1 that regions for minimum and maximum lift do not

contain load combinations with minimum drag force. It is up to the operator to determine if additional samples should be taken to populate the extremities of the design space.

4.2.1 Blocking the data points

The data points in each sub-region are randomized and divided into two blocks. Randomizing the point order before blocking the data ensures that high and low drag and lift forces are present in both blocks and do not follow a descending or ascending order. Replicates in one block are included in the other to capture block effects. All lift and drag channel responses for load combinations in one block are measured before moving on to the other block. All data for SR1 is collected before collecting SR2 data. The specific loading scheme for SR1 is shown in Table 4.2. Time between point combinations within blocks varied between 2 - 5 minutes. Block 2 data in SR1 was collected approximately 12 hours after Block 1. SR2 data was collected in a similar time frame as SR1. The techniques used to collect the data are discussed in the next chapter.

Table 4.2. Sub-Region 1 load matrix

Block	Drag Load	Lift Load	RMV Drag	RMV Lift
1	0	0	-1.91886	-3.48139
1	10.96	-21.97	-2.021	-4.56523
1	23.83	-19.71	-2.177	-4.463
1	23.06	-0.7051	-2.170	-3.512
1	14.51	-14	-2.078	-4.191
1	2.08	-8.153	-1.946	-3.912
1	5.52	-5.352	-1.983	-3.771
1	21.43	-8.979	-2.152	-3.938
1	16.62	-12.57	-2.099	-4.125
1	15.61	-3.116	-2.089	-3.652
1	12.53	-16.5	-2.061	-4.320
2	0	0	-1.915	-3.519
2	7.15	-1.564	-1.997	-3.594
2	3.78	-22.22	-1.969	-4.614
2	18.1	-16.17	-2.117	-4.310
2	19.76	-24.48	-2.143	-4.719
2	15.61	-3.116	-2.126	-3.667
2	1.99	-11.25	-1.989	-4.081
2	9	-6.35	-2.060	-3.836
2	8.31	-18.71	-2.055	-4.442
2	5.52	-5.352	-2.028	-3.789
2	0	0	-1.966	-3.523

Chapter 5

Execution Phase

The execution phase is divided into two sub-phases. First, the balance is loaded with force combinations, and lift and drag channel responses are recorded. These "primary calibration" points are used to build the math model. The second sub-phase involves collecting confirmation points by loading the force balance with combinations not included in the primary calibration process. The points are used to assess the reliability of the math models for each sub-region.

5.1 Primary calibration

Prior to calibration, a digital scale is used to ensure that the test block is oriented correctly, and the strain gages are connected to the signal conditioners. The signal conditioners are allowed to warm up, and zero-load measurements are taken once the readings from the conditioners have stabilized. The zero-force responses are the offset values that must be taken into account when using the RSM to estimate lift and drag forces. They are measured

at the beginning and end of every test block. The calibration process for each test block is as follows:

- **Step 1:** Use a digital table scale to weigh the load combinations generated via LHS. If the exact load is not obtainable, ensure that alternate loads remain in the same bin as the original loads to maintain the intended parameter distribution in the design space.

- **Step 2:** Add the weight to the containers suspended by the cables attached to the test stub. The simulated lift load will be equal to the weight hanging vertically from the test stub. Check the in-line scale to identify the horizontal load applied to the test stub, and add weight as needed to obtain the desired drag load.

- **Step 3:** Record lift and drag channel responses to the hanging calibration weights. Do not take measurements if the containers are excessively swinging, and do not touch the balance or weights while measurements are being taken. Discard measurements if an obvious outside force influences the response.

- **Step 4:** Tabulate the data. Recall that the math models express responses as functions of lift and drag. For each load combination, the operator must record lift, drag, lift channel response, and drag channel response.

- **Step 5:** Unload the force balance and repeat this process if combinations remain in the block. If all combinations in the block have been set and measured, process the data and check its quality. It is important to periodically check the quality of the data during the calibration process in case adjustments need to be made between blocks or blocks need to be repeated. For example, the author recognized that all measurements after a particular load combination were offset from previous measurements, which suggested that the force balance was loaded outside of specification, changing the zero-

load point. In the course of this work, the bounds of the calibration were adjusted to be 3 lbf to 20 lbf for drag, and 1 lbf to 20 lbf for lift.

After executing the two test blocks in SR1, a series of confirmation points were collected. Once the models are constructed, the confirmation points are estimated using the confirmation responses with the model, and the results are compared to the known values of the combinations. After collecting the confirmation points, the force balance was detached from the test section, inverted, and re-installed to load the balance with positive lift loads (SR2). The calibration set up does not allow the balance to be loaded with positive and negative lift forces in the same test block, so separate response surface models are constructed for positive and negative lift. The calibration process for the inverted balance is the same as described above. After completing the primary calibration for SR2, more confirmation points were collected.

Chapter 6

Analysis Phase

The MATLAB curve fitting application was used to generate response surface models in the form of first-order and second-order polynomials for both the lift and drag channels. Fig. 6.1 shows the first-order response surface model for the drag channel in SR2. The two models for drag and lift channels are used in conjunction to solve for lift and drag forces, because two equations are required to solve for two variables in a system of equations. During calibration, the two independent variables are the simulated lift and drag forces, and the dependent variables are the voltage readings from the lift and drag channels. Load combinations are set, and responses are measured. The relationship between loads and voltage response is represented by polynomials, so the point of calibration is to obtain the coefficients in the polynomials. Once those are obtained, unknown loads on a test article can be estimated using the coefficients and the responses to the unknown forces.

Table 6.1 contains the coefficients for the response surface models for SR2 described by the polynomial $f(x, y) = p_{00} + p_{10}x + p_{01}y$.

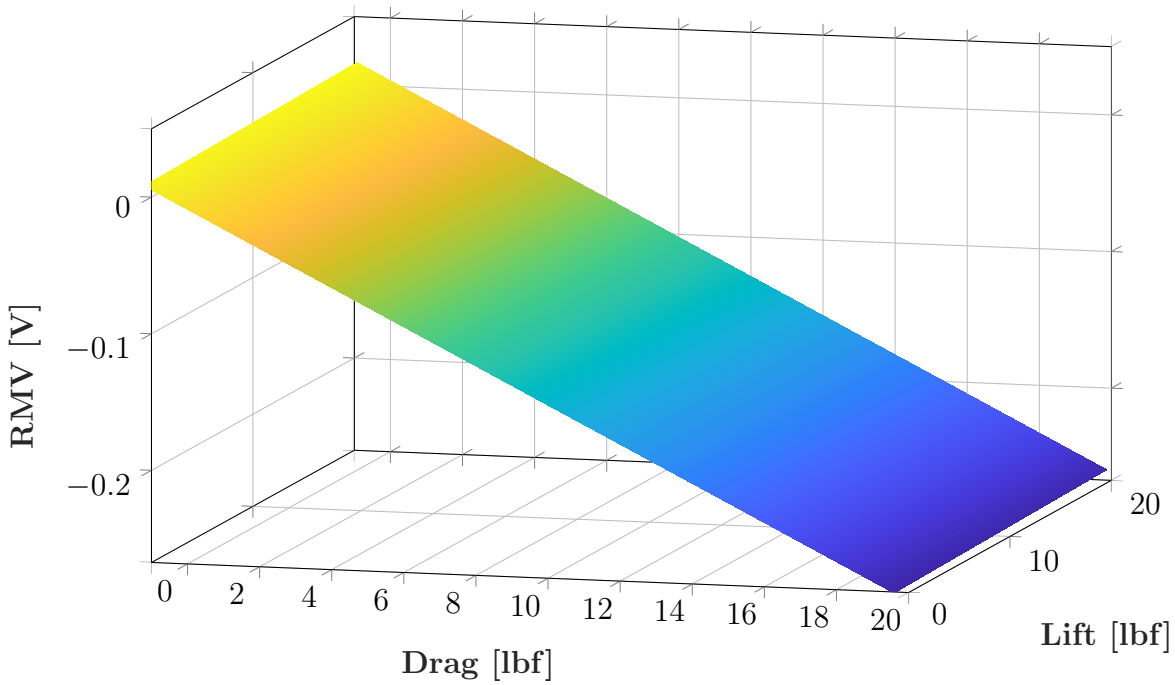

Figure 6.1. First-order RSM: SR2 Drag Channel

Table 6.1. SR2 First-Order RSM Coefficients

Coefficient	Drag Channel	Lift Channel
p_{00}	1.406e-04	1.617e-03
p_{10}	-1.328e-02	8.784e-05
p_{01}	1.957e-04	5.064e-02

To evaluate the first-order models, the channel responses from the primary calibration are used to predict lift and drag, and the predictions are compared to the known load combinations from the primary calibration. This is known as "back-calculation". Results are tabulated in Table 6.2.

Table 6.2. SR2 1^{st} Order Back Calculation Results

Metric	Drag Channel RSM	Lift Channel RSM
Mean Error [%]	1.422	1.270
Standard Error [%]	0.526	0.426
Max Error [%]	6.420	4.556
Min Error [%]	0.0165	0.395

Back calculation results for the first-order response models were compared to those of the second order models. The second-order models are described by the polynomial

$$f(x, y) = p_{00} + p_{10}x + p_{01}y + p_{20}x^2 + p_{11}xy + p_{02}y^2$$

and the coefficients and back-calculation results are recorded in Tables 6.3 and 6.4, respectively.

Table 6.3. SR2 Second Order RSM Coefficients

Coefficient	Drag Channel	Lift Channel
p_{00}	1.857e-04	1.99e-04
p_{10}	-1.273e-02	1.476e-03
p_{01}	5.044e-05	5.032e-02
p_{20}	-3.814e-05	-7.461e-05
p_{11}	2.899e-05	-7.047e-06
p_{02}	-1.246e-05	8.806e-06

Table 6.4. SR2 2^{nd} Order Back Calculation Results

Metric	Drag Channel RSM	Lift Channel RSM
Mean Error [%]	1.094	9.736
Standard Error [%]	0.386	1.875
Max Error [%]	2.897	19.18
Min Error [%]	0.212	1.078

The first-order RSM was determined to be the better RSM based on the back calculation results. The first-order model for the lift channel had lower mean, standard, maximum, and minimum errors than the second-order model. Standard error indicates how accurate the mean of a sample is compared to the true mean of the population. In this case, the "population" is the error, or residual, between estimates and true values of all possible load combinations in the design space. The standard error is a measure of how well the mean residual between back-calculation estimates and the discrete load combinations represents the true mean residual across the entire design space. Confirmation points were estimated

using the first-order models, resulting in a maximum lift and drag error of 4.63% and 3.49%, respectively. These results suggest that a second-order model over-fits the data, and the first order models should be used in hydrodynamic experiments.

Chapter 7

Flat Plate Test

Ortiz et al. investigated forces and moments on flat plates with various aspect ratios for wind turbine applications [20]. They found that the drag to lift ratio closely follows the inverse tangent of the angle of attack for nearly all measurements, and the coefficients at close proximity to the air tunnel floor are more sensitive to aspect ratio than they are in the free-stream. To check the reliability of the force balance, the balance was used to measure lift and drag forces on a wall-mounted plate at various angles of attack to compare to the Ortiz et al. results.

The test article measures 4" × 8" × 0.25". The dimensions of the plate were not arbitrary; the 8" span places the article's balance moment center at the same location as the calibration test block, the 4" chord ensures that the plate will not prevent the force balance from deflecting under high drag loads, and the resulting aspect ratio of AR = 2.0 is easily compared to the Ortiz et al. results. Brackets secure the plate to the hydrofoil rod of the force balance (Fig. 7.2). The test section was drained to set the initial angle of the plate using a digital level. All subsequent angles were set without draining the test section by loosening the clamp that secures the hydrofoil rod to the flexures of the balance and rotating the rod.

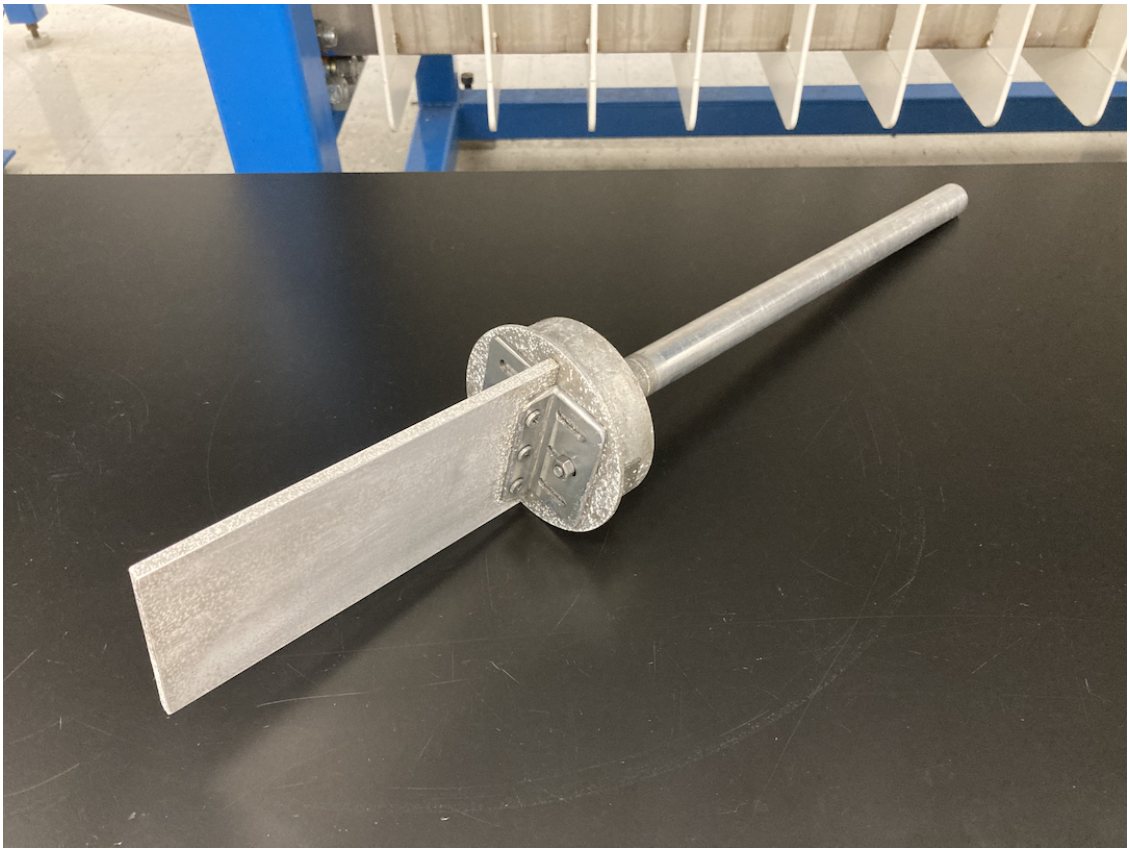

Figure 7.1. Test article secured to the central rod of the force balance

Measurements were taken at various flow speeds at angles of attack between 0° and 90°. The angle of attack was set in 5° intervals, and the flow speed order was randomized at each α level. Zero-flow measurements were taken for each α angle before measuring the response at the various flow speeds. To estimate forces with the math models, the voltage measurements from the experiment must be scaled by the ratio of the test article BMC to the calibration BMC. Because the experimental and calibration setups share the same BMC, forces on the plate are estimated without scaling the drag and lift channel responses. The response surface models for SR2 were used to estimate the lift and drag forces acting on the plate because the angles of attack and the resulting lift forces were positive. Recall that the lift channel on the force balance was calibrated from 1 lbf to 20 lbf and the drag channel was calibrated for 3 lbf to 20 lbf. Using the model to extrapolate increases error in the

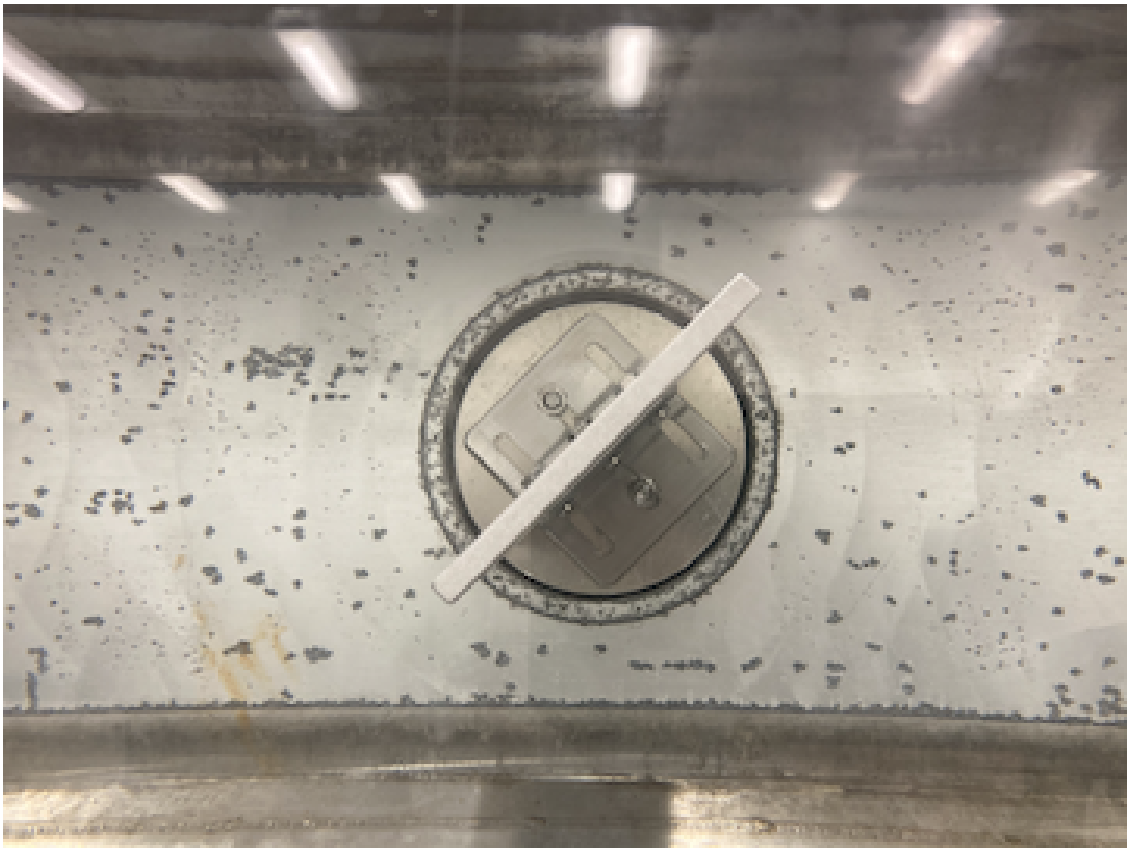

Figure 7.2. View of test article within the HSWT

predictions, so data points resulting in forces outside of the balance specifications were not considered in the comparison. Measurements at $Re = 90,800$ were compared to Ortiz et al. findings, because this flow speed allowed for the widest range of α ($20° - 70°$) based on the upper and lower force constraints of the balance, and Ortiz's Reynolds numbers varied from $Re = 60,000$ to $Re = 200,000$.

Fig. 7.3 depicts the relationship between the drag to lift ratio versus angle of attack for three plates with different aspect ratios in close proximity to a tunnel wall. Ortiz et. al. obtained the estimates for AR = 1.6 and AR = 2.5 in Fig. 7.3, and the estimates for AR = 2.0 were obtained by the author. Ortiz et. al. experimental setup involved securing a plate in a wind tunnel by using a sting to place it in close proximity to the tunnel floor [20]. The author's experimental setup differs from Ortiz's. The plate is directly mounted to the force

balance along its chord within the HSWT. Despite the different configurations, the trend in the data for AR = 2.0 follows the same trend as AR = 1.6 and AR = 2.5. The ratio of drag and lift versus angle of attack closely follows the inverse tangent of the angle of incidence (Fig. 7.3). This suggests that lift and drag predictions made with measurements from the force balance are proportionally correct.

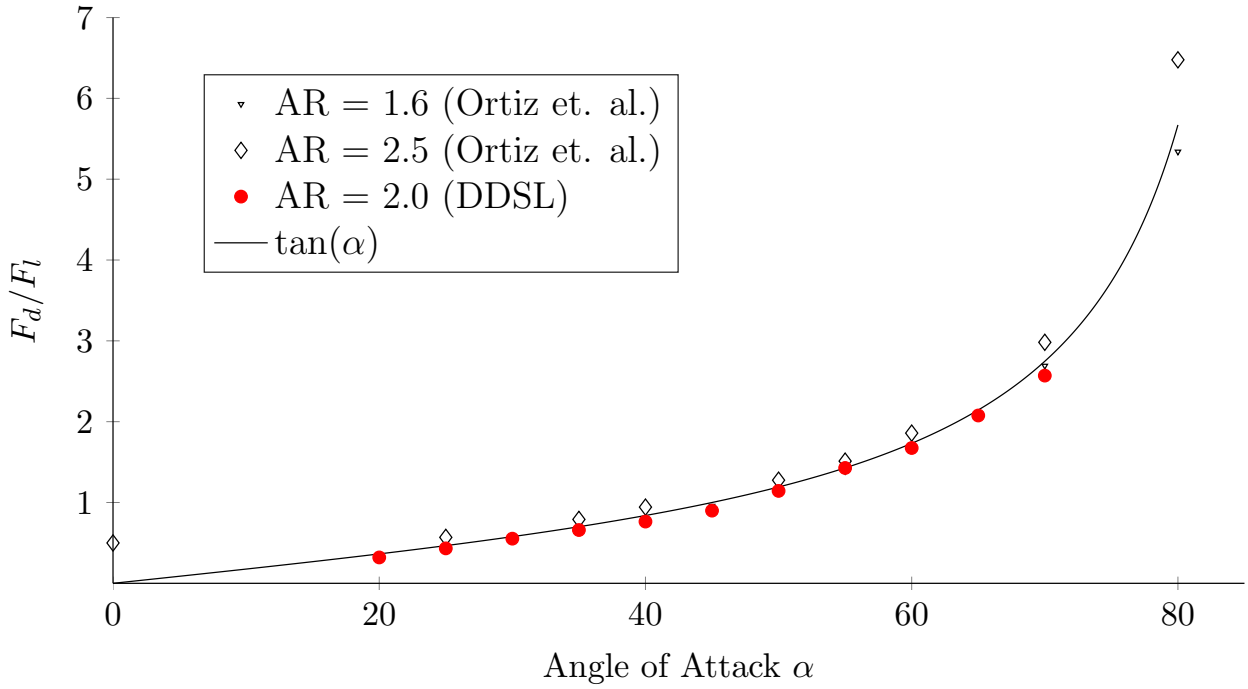

Figure 7.3. F_d/F_l vs α for various aspect ratios

The drag and lift coefficients were calculated using force estimates to determine if the balance could reliably predict the magnitude of forces applied to the plate. Figures 7.4 and 7.5 depict the drag and lift coefficients versus angle of attack. Drag and lift coefficients are described by the functions:

$$C_d = \frac{2F_d}{A\rho V^2} \tag{7.1}$$

and

$$C_l = \frac{2F_l}{A\rho V^2} \tag{7.2}$$

where F_d and F_l are drag and lift forces, respectively. The variable A is the product of the chord length and span of the plate, ρ is the density of the fluid, and V is the velocity of the fluid. A, ρ, and V are held constant for this comparison, so the coefficients change based on the forces acting on the plate. Ortiz et al. found that in all cases for plates in close proximity to a tunnel wall, drag is reduced and the main effect of AR on C_d occurs after $\alpha = 25°$ [20]. The coefficients for a plate of AR = 2.0 should fall between the coefficients for AR = 1.6 and AR = 2.5 at each angle of attack. The C_d estimate at $\alpha = 60°$ for AR = 2.0 is inconsistent with the overall trend in the data, but the majority of the data points for AR = 2.0 in Figure 7.4 follow the expected trend. Similarly, the C_l predictions for AR = 2.0 are consistently less than AR = 2.5 values and more than AR = 1.6 values (Figure 7.5).

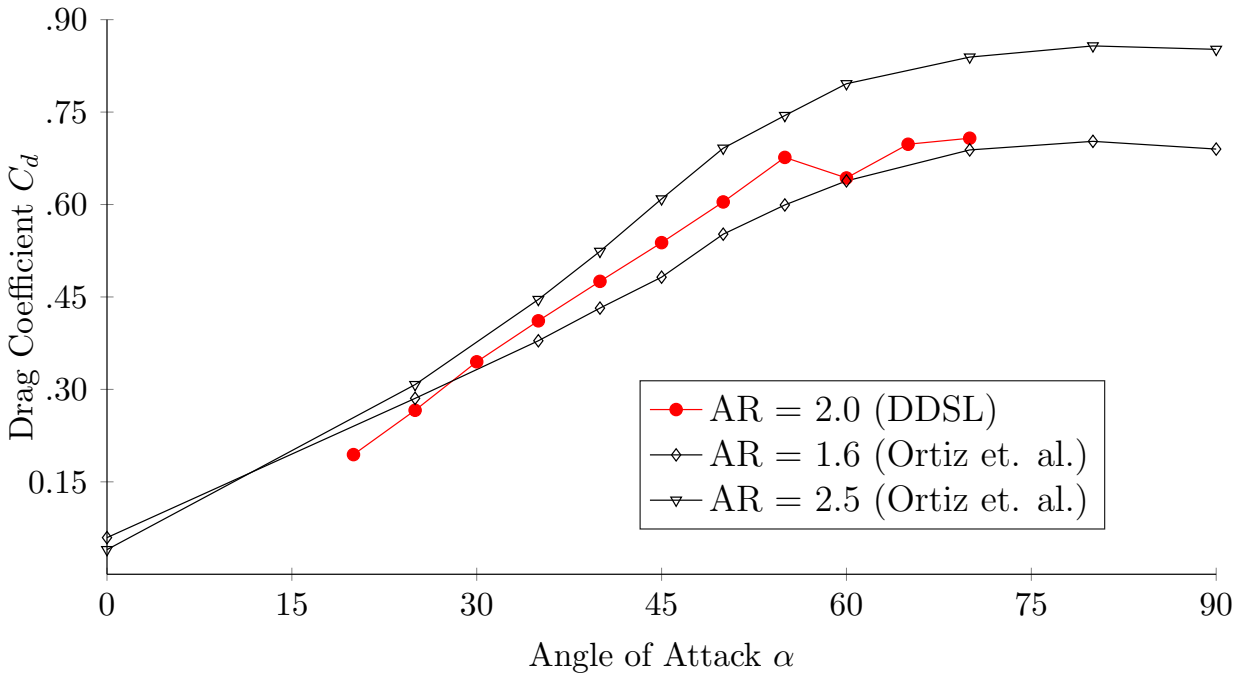

Figure 7.4. C_d versus α for various aspect ratios

The C_d and C_l versus α results in Figs. 7.4 and 7.5 suggest that the force balance can reliably predict the magnitude of forces acting on a test article during hydrodynamic experiments. The inconsistency at $\alpha = 60°$ in Figure 7.4 could possibly be due to flow

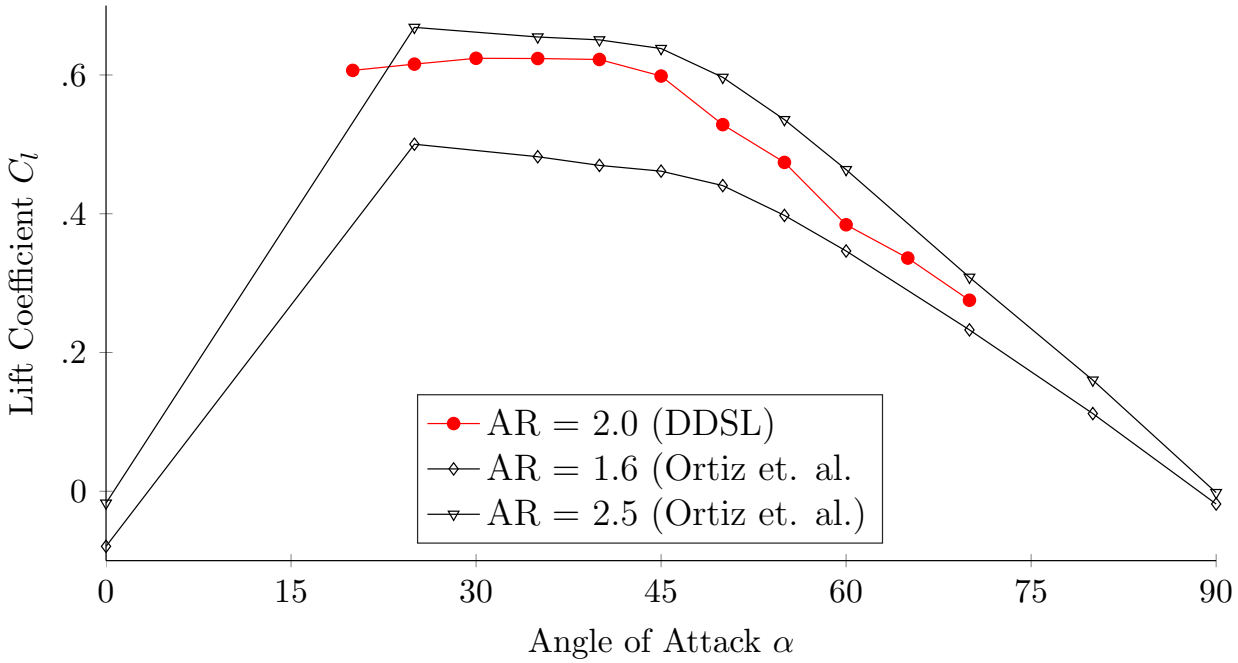

Figure 7.5. C_l versus α for various aspect ratios

interference from the bracket securing the plate to the force balance or operator error. This will be discussed further in the next chapter.

Chapter 8

Summary

8.1 Findings Summarized

Interactions between lift and drag channels on the force balance are studied by exciting both channels during calibration. The back-calculation results indicate that there is little interaction between lift and drag channels on the balance, and first-order models are adequate for estimating forces on test articles. New flexures were designed to increase the stiffness of the balance in the drag direction, and the maximum drag load was increased by 400%. The current calibration system results in an instrument that can reliably measure lift loads between ± 1 lbf and ± 20 lbf and drag loads between $+3$ lbf and $+20$ lbf to within 5% of their true value. The plate tests suggest that the models constructed with data gathered in a static calibration environment can be used to estimate forces in a hydrodynamic experiment.

8.2 Recommendations for Future Work

Water tunnel experiments can benefit from using MDOE methods. MDOE was developed to address process-oriented challenges and guard against systematic error prevalent in wind-tunnel experiments. These same issues exist in water tunnel testing, so the author suggests that experiments involving the HSWT are executed using MDOE methods. Analysis of Variance (ANOVA) tests would allow the operator to compare long-term between-block variance to shorter-term within block variance. The calibration was conducted as a two-block experiment. Decreasing the volume of data in each block and increasing the block count would facilitate higher quality ANOVA tests. The author did not determine how often the force balance should be re-calibrated, but characterizing the variance in the force balance might indicate when to re-calibrate the instrument.

The current calibration system depends on the inline scale to measure the simulated drag forces applied to the test stub. This method yielded promising results, illustrated by the plate test findings. The repeatably of the test environment is dependent on the inline scale, which is less precise than the table scale used to measure the weights added to the containers suspended by the cable system attached to the test stub. The system can be improved by designing a system that is not dependent on the inline scale. The Single-Vector Force Balance Calibration System (SVS) developed at NASA LaRC is a mechanical system that orients a force balance in such a way that the complete calibration of a six component balance is achievable with a single force vector [6]. This concept can be applied to the two-component DDSL force balance. Designing a chassis for the force balance that positions the instrument at different angles would allow both components to be calibrated by a single hanging dead weight. One can solve for the drag and lift components of the single force vector using the angle of the force balance and the magnitude of the calibration weight. This system would avoid using a pulley and inline scale to apply and measure simulated drag forces. The math

models constructed with data obtained from the pulley calibration system was less precise than specified in Equation 4.2. This is likely due to the assumption that the repeatability of the test environment was equal to the precision of the inline scale. By not using the inline scale, this assumption could be avoided.

The plate experiment can be improved by seamlessly attaching the plate to the force balance. In the experiment described above, the plate is secured to the balance with brackets and bolts that protrude into the test section. This changes the geometry of the test article and influences fluid flow about the plate. Although the results follow trends in the literature, estimates might be improved by eliminating the hardware that secures the plate to the balance. An alternate approach might be designing a system that places the plate in the free stream. The forces acting on the member that connects the plate to the balance would need to be measured, but this set-up would eliminate wall effects on the test article.

Bibliography

[1] H. Curtis, *Operation and Maintenance of a High-Speed Water Tunnel*. Master's thesis, University of Georgia, 2018.

[2] I. Nedyalkov, *Design of contraction, test section, and diffuser of a high-speed water tunnel*. Master's thesis, Chalmers University of Technology, 2012.

[3] R. Etter and M. Wilson, "The large cavitation channel," *Proc. 23rd American Towing Tank Conference (New Orleans, LA)*, 1992.

[4] T. H. Johnson, P. A. Parker, and D. Landman, "Calibration designs for non-monolithic wind tunnel force balances," *Journal of Aircraft*, vol. 47, no. 6, 2010.

[5] I. B. T. W. Group, "Recommended practice: Calibration and use of internal strain-gage balances with application to wind tunnel testing (aiaa r-091-2003)," 2003.

[6] P. Parker, M. Morton, and W. L. Draper, "A single-vector force calibration method featuring the modern design of experiments (invited)," *39th Aerospace Sciences Meeting and Exhibit*, 2001.

[7] M. Robinson, J. M. Schramm, and K. Hannemann, "An investigation into internal and external force balance configurations for short duration wind tunnels," *Spacecraft Section, German Aerospace Center*, vol. 96, pp. 129–136, 2006.

[8] R. DeLoach, "Applications of modern experiment design to wind tunnel testing at nasa langley research center," *AIAA Journal*, vol. 20, p. 2884, 1998.

[9] R. DeLoach, "Tailoring wind tunnel data volume requirements through the formal design of experiments," *20th AIAA Advanced Measurement and Ground Testing Technology Conference*, 1998.

[10] R. DeLoach, "Blocking: a defense against long-period unexplained variance in aerospace ground testing," in *41st Aerospace Sciences Meeting and Exhibit*, p. 650, 2003.

[11] R. DeLoach and J. Micol, "Comparison of resource requirements for a wind tunnel test designed with conventional vs. modern design of experiments methods," in *49th AIAA Aerospace Sciences Meeting including the New Horizons Forum and Aerospace Exposition*, 2011.

[12] R. DeLoach, "Improved quality in aerospace testing through the modern design of experiments," in *38th Aerospace Sciences Meeting and Exhibit*, p. 825, 2000.

[13] R. DeLoach, J. Hill, and W. Tomek, "Practical applications of response surface methods in the national transonic facility," in *39th Aerospace Sciences Meeting and Exhibit*, p. 167, 2001.

[14] R. DeLoach, "Tactical defenses against systematic variation in wind tunnel testing," in *40th AIAA Aerospace Sciences Meeting & Exhibit*, p. 885, 2002.

[15] R. DeLoach, "Putting ten pounds in a five-pound sack: Configuration testing with mdoe," in *21st AIAA Applied Aerodynamics Conference*, p. 4212, 2003.

[16] J. F. Box, "Sir Ronald Fisher and the design of experiments, 1922–1926," *The American Statistician*, vol. 34, no. 1, pp. 1–7, 1980.

[17] R. Therrien, S. Roux, B. Comtois, and M. Wosnik, "Design of a high speed water tunnel force balance and testing of high performance hydrofoils for marine hydrokinetic turbines," 2012.

[18] C. Wieselsberger, "New data on the laws of fluid resistance," *Physikalische Zeitschrift*, vol. 22, no. 4, 1922.

[19] A. Giunta, S. Wojtkiewicz, and M. Eldred, "Overview of modern design of experiments methods for computational simulations," in *41st Aerospace Sciences Meeting and Exhibit*, p. 649, 2003.

[20] X. Ortiz, D. Rival, and D. Wood, "Forces and moments on flat plates of small aspect ratio with application to pv wind loads and small wind turbine blades," *Energies*, vol. 8, no. 4, pp. 2438–2453, 2015.